Analysis and Characterization of Ultrawide-Band Scalar Volume Sources and the Fields They Radiate: Part II—Square Pulse Excitation

Edwin A. Marengo, *Member, IEEE*, Anthony J. Devaney, *Member, IEEE*, and Ehud Heyman, *Senior Member, IEEE*

***Abstract*—In a previous paper [1], we studied transient radiation from scalar collimated volume source distributions subjected to impulsive excitation. In this paper, we extend our analysis and results to the case of nonimpulsive excitation, paying special attention to the parameterization of the radiation pattern of three-dimensional (3-D) ellipsoid source distributions driven by square pulses of finite duration. We study the role both of the source's space distribution and of the square pulse duration on the generation of well-collimated short-pulse fields. In particular, we explore the source's angular and range resolutions as functions of the transverse and longitudinal dimensions of the source (for a fixed source volume) and of the pulse duration.**

***Index Terms*—Transient propagation.**

I. Introduction

In a previous paper [1] we investigated the radiation properties of scalar wave fields $U(\mathbf{r},t)$ radiated by three-dimensional (3-D) sources to the scalar wave equation

$$\left(\nabla^2 - \frac{1}{c^2}\frac{\partial^2}{\partial t^2}\right)U(\mathbf{r},t) = -4\pi Q(\mathbf{r},t) \tag{1}$$

paying special attention to sources $Q(\mathbf{r},t)$ having the space-time separable form of a "traveling wave"

$$Q(\mathbf{r},t) = q_0(\mathbf{r})G(t - \hat{\mathbf{z}}\cdot\mathbf{r}/c) \tag{2}$$

where, without loss of generality, the main beam direction was chosen to be the positive z axis $(\hat{\mathbf{z}})$ and the space distribution $q_0(\mathbf{r})$ was normalized so that

$$\int d\mathbf{r}' q_0(\mathbf{r}') = 1. \tag{3}$$

In order to compare the radiation performance for different source parameters we have considered the source's volume V as invariant.

The class of sources defined in (2) represents a distribution of nondispersive isotropic point radiators, all of which radiate the same time signature $G(t)$ but with space-dependent strength $q_0(\mathbf{r})$. The source defined in (2) could represent a discrete collection of point radiators (e.g., a 3-D antenna array of isotropic radiating elements) or a spatially continuous distribution of such radiators (note that in the discrete realization, the spectral shaping of the far field is also affected by the interelement spacings). A special case of such distribution is a uniformly distributed source wherein all point radiators are driven with the same strength: specific examples of uniform parallelepiped source distributions have been considered in [1].

In the present paper, we explore uniform ellipsoidal source distributions whose axis coincide with the z axis in (2) for which closed-form expressions can be obtained for all radiation directions and for all observation times. Furthermore, since the ellipsoidal shape may be continuously changed from a prolate to an oblate spheroidal shape, the closed-form results explain the different radiation characteristics of both elongated, quasi-linear traveling wave source distributions and quasi-planar broadside pulsed distributions, as well as those of 3-D sources with comparable longitudinal and transverse dimensions. Finally, while the analysis in [1] has concentrated on impulsive sources [i.e., $G(t) = \delta(t)$ in (2)], which generate near the beam axis singular field terms that cannot be parameterized, the emphasis here is placed on finite pulses (specifically on square pulses).

Our interest in the source distributions considered above arises from the fact that they yield highly collimated pulse beam fields with high degree of angular and range resolutions when they are driven by very short pulses $G(t)$ [1]. Motivation for the source structure in (2) is also provided by the possibility of building 3-D pulsed antenna arrays composed of identical electrically small photoconducting elements [2]–[4]. These antennas, made of III–V compound semiconductor wafers, radiate microwave pulses when triggered by short duration (e.g., picosecond) optical pulses. A 3-D array of such photoconducting elements can thus be realized using fiber optics and optical splitters, the latter to control the excitation strength associated with each element as dictated by $q_0(\mathbf{r})$ in (2) (the excitation strength can also be controlled by the voltage bias applied to each element [2], [3]). The progressive time delay in (2) can be controlled either by a delay network or simply by taking advantage of the propagation delay of the exciting optical wavefront along the z axis [5]. In addition, the antenna arrays described above are expected to have reduced microwave interelement coupling due to the short periods of photoconductivity associated with each element [5].

Manuscript received September 25, 1996; revised October 3, 1997. This work was supported in part by the U.S. Air Force Office of Scientific Research, Boling AFB, Washington, DC, under Grant F49620-93-1-0093, by the Center for Electromagnetics Research, Northeastern University, Boston, MA, and by the Israel Science Foundation under Grant 574/95.

E. A. Marengo and A. J. Devaney are with the Department of Electrical and Computer Engineering, Northeastern University, Boston, MA 02115 USA.

E. Heyman is with the Department of Electrical Engineering and Physical Electronics, Tel Aviv University, Tel Aviv, 69978 Israel.

Publisher Item Identifier S 0018-926X(98)01493-8.

The source model defined in (2) can thus be viewed as an approximation to a 3-D distribution of electrically small (and thereby quasi-isotropic) photoconducting elements excited by a space-dependent amplitude $q_0(\mathbf{r})$ and with progressive time delay $\hat{\mathbf{z}} \cdot \mathbf{r}/c$ along the main beam direction $\hat{\mathbf{z}}$.

This paper generalizes our work in [1] by considering transient radiation from volume source distributions excited by finite duration square pulses. Our goal is to explore the role both of the excitation pulse duration W and of the length-to-width ratio $\ell \equiv L/a$ (where L and a are, respectively, the longitudinal and transverse dimensions of the source distribution) in establishing a highly collimated pulsed field with a high degree of angular and range resolutions. The angular resolution will be quantified from the directional properties of the *time-domain radiation pattern* $F(\hat{\mathbf{r}}, t)$ characterized by the peak amplitude and energy patterns while the range resolution will be determined from the pulse duration of $F(\hat{\mathbf{r}}, t)$. Special emphasis will be placed on the far-field properties near the main beam direction.

The work reported here encompasses that of Harmuth [6] where the peak amplitude, energy, and slope patterns of a linear (one-dimensional) array composed of elements that radiate far-field square pulses are derived using simple geometrical arguments. Also, the Radon transform radiation integral, which is the starting point of the present analysis, is a special case of the theory in [7] (formulated for electromagnetic sources) that applies to any time-dependent source distribution [not necessarily of the form in (2)]. We would also like to mention that even though we restrict our attention to ellipsoidal volume source distributions, the formulation presented here is rather general and can be applied to any 3-D source configuration of the form in (2). In what follows, we adopt the notation used in [1].

II. Review of the General Theory

The time-domain radiation pattern $F(\hat{\mathbf{r}}, t)$ is obtained by asymptotically evaluating the radiation field $U(\mathbf{r}, t)$ as $r \to \infty$, thus yielding [7], [8]

$$U(r\hat{\mathbf{r}}, t) \sim \frac{1}{r} F(\hat{\mathbf{r}}, t - r/c). \tag{4}$$

For the special case of the source in (2), $F(\hat{\mathbf{r}}, t)$ reduces to [1]

$$F(\hat{\mathbf{r}}, t) = G(t) * F_0(\hat{\mathbf{r}}, t) \tag{5}$$

where $*$ is used to denote temporal convolution and where the *time-domain pulsed-radiation pattern* $F_0(\hat{\mathbf{r}}, t)$ (e.g., the source's impulse response) is given by [1]

$$F_0(\hat{\mathbf{r}}, t) = \frac{c}{\xi} \overline{q_0}(\hat{\boldsymbol{\xi}}, s)\Big|_{s=-ct/\xi} \tag{6}$$

where $\boldsymbol{\xi} = \xi\hat{\boldsymbol{\xi}} = \hat{\mathbf{r}} - \hat{\mathbf{z}}$ (hence, $\xi = 2\sin\theta/2$) and $\overline{q_0}(\hat{\boldsymbol{\xi}}, s)$ is the Radon transform of $q_0(\mathbf{r})$ evaluated at the plane $\mathbf{r} \cdot \hat{\boldsymbol{\xi}} = s$. Thus, for fixed $\hat{\mathbf{r}}$, the time-domain pulsed-radiation pattern $F_0(\hat{\mathbf{r}}, t)$ is defined by the projection of $q_0(\mathbf{r})$ onto the line directed along the unit vector $\hat{\boldsymbol{\xi}}$.

A schematization of (6) is depicted in Fig. 1, which shows the planes $\mathbf{r} \cdot \hat{\boldsymbol{\xi}} = s$ that lie perpendicular to the unit vector

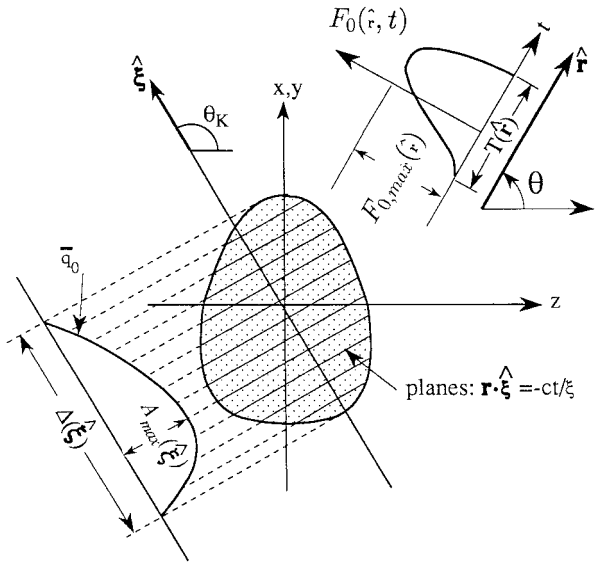

Fig. 1. Schematization of (6). $\overline{q_0}(\hat{\boldsymbol{\xi}}, s)$ is the Radon transform along the $\hat{\boldsymbol{\xi}}$ axis obtained by integrating $q_0(\mathbf{r})$ on surfaces orthogonal to $\hat{\boldsymbol{\xi}}$. The time-domain pulsed-radiation pattern $F_0(\hat{\mathbf{r}}, t)$ is related to $\overline{q}_0$ via the scaling in (6).

$\hat{\boldsymbol{\xi}}$ along which the projection is computed. $\overline{q_0}(\hat{\boldsymbol{\xi}}, s)$ is shown in the left portion of the figure as the plot of the area of q_0 computed along the planes $\mathbf{r} \cdot \hat{\boldsymbol{\xi}} = s$ with s being a parameter along the $\hat{\boldsymbol{\xi}}$ axis. The time-domain pulsed-radiation pattern is shown in the right portion of the figure and is obtained from $\overline{q_0}(\hat{\boldsymbol{\xi}}, s)$ by mapping $s \to -ct/\xi$ and scaling the amplitude by c/ξ. Referring to Fig. 1, we see that if the source dimension in the $\hat{\boldsymbol{\xi}}$ direction is $\Delta(\hat{\boldsymbol{\xi}})$, then the pulse duration of $F_0(\hat{\mathbf{r}}, t)$ along the observation direction $\hat{\mathbf{r}}$ is

$$T(\hat{\mathbf{r}}) = \xi\Delta(\hat{\boldsymbol{\xi}})/c. \tag{7}$$

Similarly, the temporal peak amplitude—defined as the maximum amplitude (over all time t) of the time-domain pulsed-radiation pattern $F_0(\hat{\mathbf{r}}, t)$ in a given direction—is given by

$$F_{0,\max}(\hat{\mathbf{r}}) = c|A_{\max}(\hat{\boldsymbol{\xi}})|/\xi \tag{8}$$

where $A_{\max}(\hat{\boldsymbol{\xi}})$ is the maximum projection of the source's space distribution $q_0(\mathbf{r})$ onto the $\hat{\boldsymbol{\xi}}$ axis.

III. Time-Domain Pulsed-Radiation Pattern: Ellipsoid Distributions

We consider uniform volume-source distributions $q_0(\mathbf{r})$ with the shape of an ellipsoid that has rotational symmetry with respect to the z axis and with radial and axial dimensions a and L, respectively. To comply with the source normalization in (3), the source's magnitude is taken to be

$$q_0(\mathbf{r}) = \begin{cases} 1/V, & \frac{x^2+y^2}{a^2} + \frac{z^2}{L^2} \le \frac{1}{4} \\ 0, & \text{else} \end{cases} \tag{9}$$

with $V = \frac{\pi}{6} a^2 L$ being the source's volume. Henceforth, we shall express the source dimensions a and L in terms of the volume V and the length-to-width ratio $\ell \equiv L/a$. Thus, $a = (6/\pi)^{1/3} V^{1/3} \ell^{-1/3}$ and $L = (6/\pi)^{1/3} V^1 \ell^{2/3}$. By doing this we may now compare sources with the same volume

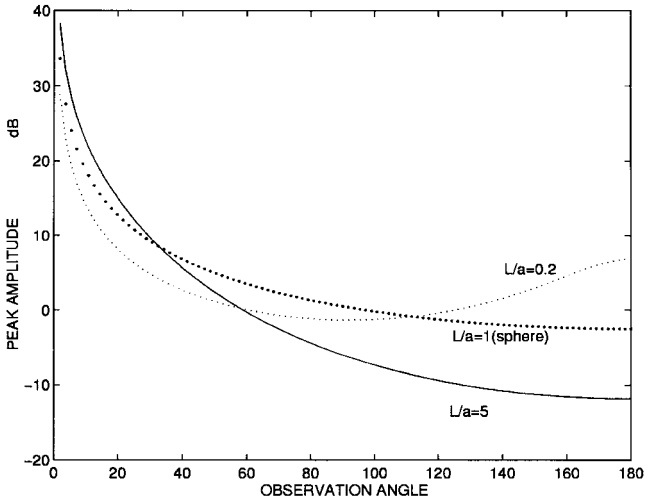

Fig. 2. Peak amplitude pattern of ellipsoidal source distributions under impulsive excitation $F_{0,\max}$ as function of θ (in degrees) for $\ell = 0.2, 1, 5$.

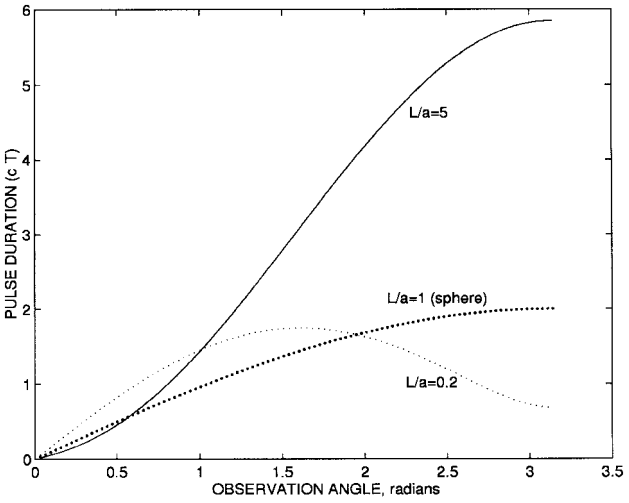

Fig. 3. Far-field pulse duration T of ellipsoidal source distributions under impulsive excitation versus θ (in radians) for $\ell = 0.2,\ 1,\ 5$.

V (and thereby the same input energy[1]) for different values of the parameter ℓ. Furthermore, when comparing elongated sources ($\ell > 1$) with flat sources ($\ell < 1$), we shall consider, in particular, sources with the same maximum dimension defined as the diameter of the smallest sphere completely enclosing the source. Therefore, we shall compare the results for an elongated source with, say, $\ell = \ell_e > 1$ with those of a flat source with $\ell = \ell_e^{-2}$.

Using the general Radon transform relation in (6), it is found in the Appendix that the time signature of $F_0(\hat{\mathbf{r}}, t)$ for the ellipsoidally shaped distribution in (9) has, at a given observation direction $\hat{\mathbf{r}}$ with polar angle θ, the shape of a parabola

$$F_0(\theta, t) = \begin{cases} \frac{3}{2T(\theta)} - \frac{6}{[T(\theta)]^3} t^2 & |t| \le \frac{1}{2} T(\theta) \\ 0, & \text{else} \end{cases} \tag{10}$$

where

$$T(\theta) = c^{-1}(6/\pi)^{1/3} \ell^{-1/3} V^{1/3} \sin\theta \sqrt{1 + \ell^2 \tan^2(\theta/2)} \tag{11}$$

is the time duration of $F_0(\theta, t)$. The peak amplitude $F_{0,\max}(\theta)$ is readily seen from (10) to be (see Appendix)

$$F_{0,\max}(\theta) = \max_t [|F_0(\theta, t)|] = \frac{3}{2T(\theta)}. \tag{12}$$

Following the discussion in [1], we define the energy radiation pattern

$$S(\hat{\mathbf{r}}) = \pi \int_{-\infty}^{\infty} dt |F(\hat{\mathbf{r}}, t)|^2 = \int_0^{\infty} d\omega |f(\hat{\mathbf{r}}, \omega)|^2 \tag{13}$$

where $f(\hat{\mathbf{r}}, \omega)$ is the frequency-domain radiation pattern, i.e., the temporal Fourier transform of $F(\hat{\mathbf{r}}, t)$. Thus, the energy radiation pattern of ellipsoid distributions subjected to impulsive excitation is found to be

$$S(\theta) = \frac{6\pi}{5T(\theta)} \tag{14}$$

[1]Valid for sources of the form (2) that are uniformly excited.

hence, the peak amplitude radiation pattern $F_{0,\max}(\theta)$ and the energy radiation pattern $S(\theta)$ under impulsive excitation are identical within a multiplicative factor.

In the limit $\theta \to 0$ we obtain from (11)

$$T(\theta) \sim (6/\pi)^{1/3} V^{1/3} \ell^{-1/3} \theta / c \tag{15}$$

hence, $T(\theta)$ *decreases* monotonically with ℓ (for fixed $\theta \simeq 0$), while from (12), (14), (15), both $F_{0,\max}(\theta)$ and $S(\theta)$ *increase* monotonically with ℓ. Under impulsive excitation, elongated (large ℓ) sources thus produce far-field pulses of higher amplitude and shorter duration in the main-beam direction $\theta \simeq 0$.

Fig. 2 shows plots of the peak amplitude radiation pattern $F_{0,\max}(\theta)$ for ellipsoid source distributions with length-to-width ratios $\ell = 5,\ 1$, and 0.2. These plots reveal that for a given $\theta \simeq 0$, higher radiated energy and peak amplitude (and thereby peak power) is available for larger ℓ (i.e., elongated distribution case). The presence of a secondary radiation lobe at $\theta = \pi$ for the small ℓ (planar source) case is also observed. Plots of the pulse duration $T(\theta)$ for the cases $\ell = 5,\ 1$, and 0.2 are shown in Fig. 3. We found that the θ dependence of the pulse duration is monotonic only for $\ell \le 1$ and, more importantly, that the pulse duration for a fixed θ in the vicinity of the main-beam axis (i.e., $\theta \simeq 0$) is shorter for larger ℓ. For physical interpretation of the abovementioned effects, the interested reader is referred to [1].

IV. Time-Domain Radiation Pattern Under Square-Pulse Excitation

In this section, we investigate the properties of the time-domain radiation pattern generated by scalar ellipsoid source distributions driven by unit amplitude square pulses having time duration W, i.e.,

$$G(t) = \begin{cases} 1, & 0 \le t \le W \\ 0, & \text{otherwise.} \end{cases} \tag{16}$$

We shall present the results in terms of the normalized pulse duration

$$\bar{W} = cW/V^{1/3}. \tag{17}$$

The time-domain radiation pattern $F(\hat{\mathbf{r}},t)$ is now computed by convolving the square pulse $G(t)$ of (16) with the time-domain pulsed-radiation pattern $F_0(\theta,t)$ of (10) and (11). In performing the convolution, one identifies two distinct angular domains $\theta \le \Theta_c(\ell,\bar{W})$ and $\theta \ge \Theta_c(\ell,\bar{W})$ where

$$\Theta_c(\ell,\bar{W}) = 2\sin^{-1}\left[\frac{-1+\sqrt{1+(\pi/6)^{2/3}\ell^{2/3}(\ell^2-1)W^2}}{2(\ell^2-1)}\right]^{1/2}. \tag{18}$$

For $(\pi/6)^{2/3}\ell^{2/3}(\ell^2-1)\bar{W}^2 \ll 1$ this expression yields

$$\Theta_c(\ell,\bar{W}) = 2\sin^{-1}\left[\frac{1}{2}\left(\frac{\pi}{6}\right)^{1/3}\ell^{1/3}\bar{W}\right]. \tag{19}$$

This approximation also provides the limit of (18) at $\ell = 1$. Θ_c is defined by the condition that for $\theta < \Theta_c$, $T(\theta) < W$ while for $\theta > \Theta_c$, $T(\theta) > W$ where $T(\theta)$ is defined in (11). Accordingly, for $\theta < \Theta_c$ there is a time interval denoted as $T/2 < t < W - T/2$ where

$$G(t) * F_0(\theta,t) = \int dt\, F_0(\theta,t) = \int d\mathbf{r}' q_0(\mathbf{r}') = 1 \tag{20}$$

where we have also used the normalization in (3). By manipulating the convolution $G(t) * F_0(\theta,t)$ separately in these two angular regions we obtain (21), shown at the bottom of the page, for $\theta \le \Theta_c$ and (22), shown at the bottom of the page, for $\theta \ge \Theta_c$. From (11), $T(\theta = 0) = 0$. Hence, from (21), $F(\theta = 0, t) = G(t)$ as expected.

A. Peak-Amplitude Pattern

The peak-amplitude radiation pattern $F_{\max}(\theta)$ is found from (21)–(22) to be

$$F_{\max}(\theta) = \max_t[|F(\theta,t)|] = \begin{cases} 1 & \theta \le \Theta_c \\ \frac{3W}{2T(\theta)} - \frac{W^3}{2[T(\theta)]^3} & \theta \ge \Theta_c. \end{cases} \tag{23}$$

Note that in the small W limit, (23) yields $F_{\max}(\theta) \sim \frac{3W}{2T(\theta)}$, which agrees with the impulsive excitation result (12) (apart from the factor W arising from the fact that in the square pulse case $\int dt\ G(t) = W$).

Fig. 4(a)–(f) explores the combined role of the pulse width W and of the radiator shape on the peak amplitude radiation pattern $F_{\max}(\theta)$. The figure shows plots of $F_{\max}(\theta)$ for $\ell = 100, 10, 1$ (sphere), 0.1, and 0.01 and for various normalized pulse durations $\bar{W}$ [see (17)]. Note the angular region near the beam axis where $F_{\max} = 1$, which is more visible for the large W case. As expected, high directivity is obtained in the large or small ℓ limits. This result is related, of course, to the overall linear dimension of the source distribution (i.e., the diameter of the smallest sphere completely enclosing the source), which becomes increasingly larger for $\ell \gg 1$ and $\ell \ll 1$. The plots also provide insight into the need for excitation pulses of short duration (relative to the source's size) in order to achieve good angular resolution.

B. Peak-Amplitude Beamwidth: Θ_c

In order to explore the effect of ℓ and $\bar{W}$ on the beamwidth, we shall refer to the angle Θ_c defined in (18). From (23) this angle is readily identified as the 0-dB beamwidth. We have also studied numerically the behavior of the 3-dB beamwidth of the peak-amplitude radiation pattern $F_{\max}(\theta)$, but the results (not shown) where similar to those obtained for Θ_c.

We consider first the limiting case $\bar{W} \ll 1$ (*quasi-impulsive* excitation). In this case, we obtain from (18)

$$\Theta_c(\ell,\bar{W})|_{\bar{W}\to 0} \sim (\pi/6)^{1/3}\ell^{1/3}\bar{W}. \tag{24}$$

For large planar sources ($\ell \ll 1$), this approximation is valid if $\ell\bar{W}^3 \ll 6/\pi$, while for large elongated sources ($\ell \gg 1$), it is valid if $\ell\bar{W}^{3/4} \ll (6/\pi)^{1/4}$. Thus, under these conditions the flat sources are seen to yield better peak amplitude directivity than the elongated ones. Note also that the impulsive excitation limit ($\bar{W} = 0$) yields $\Theta_c = 0$ independently of ℓ. This, of course, is in agreement with results reported in [1], where the normalized peak amplitude radiation patterns of elongated and planar sources were found to exhibit identical angular dependence in the vicinity of the main beam direction.

The condition in (24) applies for both elongated and flat sources as long as the excitation pulse is short enough as specified above. Another possible limit is for a large elongated source ($\ell \gg 1$) excited by a relatively long pulse such that $\ell\bar{W}^{3/4} \gg 1$. In this case (19) yields

$$\Theta_c(\ell,\bar{W}) \simeq \sqrt{2}(\pi/6)^{1/6}\ell^{-1/3}\bar{W}^{1/2} \tag{25}$$

which tends to zero as $\ell \to \infty$ subject to the condition $\ell\bar{W}^{3/4} \gg 1$.

Fig. 5 shows plots of Θ_c versus ℓ and parameterized by different values of $\bar{W}$. For a fixed $\bar{W}$, there is a value of ℓ (say ℓ_0) where Θ_c reaches a maximum and the angular resolution is poorest (for a source with a given volume and pulse length).

$$F(\theta,t) = \begin{cases} \frac{1}{2} + \frac{3}{2T}t - \frac{2}{T^3}t^3 & -T/2 \le t \le T/2 \\ \int dt\, F_0(\theta,t) = 1 & T/2 \le t \le W - T/2 \\ \frac{1}{2} + \frac{3}{2T}(W-t) - \frac{2}{T^3}(W-t)^3 & -T/2 + W \le t \le T/2 + W \end{cases} \tag{21}$$

$$F(\theta,t) = \begin{cases} \frac{1}{2} + \frac{3}{2T}t - \frac{2}{T^3}t^3 & -T/2 \le t \le W - T/2 \\ \frac{3W}{2T} - \frac{2}{T^3}(W^3 - 3W^2t + 3Wt^2) & W - T/2 \le t \le T/2 \\ \frac{1}{2} + \frac{3}{2T}(W-t) - \frac{2}{T^3}(W-t)^3 & T/2 \le t \le W + T/2 \end{cases} \tag{22}$$

Note also that for large $\bar{W}$'s, there is a range of ℓ where Θ_c reaches its maximal possible value π so that the source does not exhibit any peak-amplitude directivity.

We also explored analytically the variation of ℓ_0 with $\bar{W}$ using (18), thus finding that ℓ_0 decreases monotonically with $\bar{W}$. Moreover, $\ell_0 \to \infty$ as $\bar{W} \to 0$ (quasi-impulsive case). Hence, optimal selection of the shape of the radiator is accomplished in the quasi-impulsive case ($\bar{W} \to 0$) by using the smallest possible value of ℓ (i.e., a planar source).

C. Energy and Correlation Patterns

Next, we shall explore the directional dependence both of the energy radiation pattern [defined in (13)] and of a radiation characterization we shall call the "correlation" or "matched filter" pattern $L(\theta)$, which we define as

$$L(\theta) = \frac{\max_t[|F(\theta,t) * F(\theta=0,t)|]}{\max_t[|F(\theta=0,t) * F(\theta=0,t)|]} \tag{26}$$

where $*$ denotes temporal convolution. $L(\theta)$ provides a measure of the directional dependence of the (normalized) peak amplitude at the output of a matched filter tuned to the far-field pulse in the main-beam direction $F(\theta=0,t) = G(t)$ (where a target or receiver may be expected to be located). This characterization thus simulates the angular resolution available in target detection or secure communication applications.

The normalized energy radiation pattern $\bar{S}(\theta) = S(\theta)/S(\theta=0) = \frac{S(\theta)}{\pi W}$ is obtained from (13), (21), and (22) and is given by

$$\bar{S}(\theta) = 1 - \frac{9}{35W}T \tag{27}$$

for $\theta \le \Theta_c$, where $T(\theta)$ is given in (11), and by

$$\bar{S}(\theta) = \frac{6}{5}\frac{W}{T} - \left(\frac{W}{T}\right)^3 + \frac{3}{5}\left(\frac{W}{T}\right)^4 - \frac{2}{35}\left(\frac{W}{T}\right)^6 \tag{28}$$

for $\theta \ge \Theta_c$. (We normalize S so as to be able to compare sources excited by pulses of different duration.)

The "correlation pattern" $L(\theta)$ is obtained from (26), (21), and (22), giving

$$L(\theta) = \begin{cases} 1 - \frac{3}{16W}T(\theta), & \theta \le \Theta_{cL} \\ \frac{3}{2T(\theta)}W - \frac{1}{[T(\theta)]^3}W^3, & \theta \ge \Theta_{cL} \end{cases} \tag{29}$$

where Θ_{cL} is defined by $T(\Theta_{cL}) = 2W$.

1) Special Case: Quasi-Impulsive Excitation: Consider first the limit $\bar{W} \ll 1$. We examine this case using the small W limits of $\bar{S}(\theta)$ and $L(\theta)$ as computed using (27), (28), and (29). Here, $\Theta_c \ll 1$ as described in (24). We use the small θ approximations of $T(\theta)$ from (15). For $\theta \le \Theta_c$ we therefore obtain from (27), with (15) and (24)

$$\bar{S}(\theta) \simeq 1 - \frac{9}{35}\left(\frac{6}{\pi}\right)^{1/3}\ell^{-1/3}\bar{W}^{-1}\theta = 1 - \frac{9}{35}\frac{\theta}{\Theta_c}. \tag{30}$$

This expression describes $\bar{S}(\theta)$ near the beam axis for $\theta \le \Theta_c$ but, as follows from the second expression in (30), it does not describe the relevant range for $\theta > \Theta_c$ where $\bar{S}(\theta)$ may still be nonnegligible [note that $\bar{S}(\Theta_c)$ is about 0.75 of the value of $\bar{S}$ at $\theta = 0$]. Hence, the effective beamwidth of the energy pattern will be found from the analysis of $\bar{S}$ in the region $\theta \ge \Theta_c$ where $\bar{S}$ is described by (28). The leading term (in W) in this expression is given by $\bar{S}(\theta) \simeq \frac{6W}{5T} \simeq \frac{6}{5}\left(\frac{\pi}{6}\right)^{1/3}\ell^{1/3}\theta^{-1}\bar{W}$, where the second approximation follows from (15). The 3-dB beamwidth obtained by solving $\bar{S}(\theta) = \frac{1}{2}$ is therefore given by

$$\theta_{3\,\mathrm{dB}} = \frac{12}{5}\left(\frac{\pi}{6}\right)^{1/3}\ell^{1/3}\bar{W} = \frac{12}{5}\Theta_c \tag{31}$$

and is smaller for flat sources (small ℓ). One therefore concludes that flat sources provide better energy focusing than elongated sources of comparable volume. Note in addition that since $S(\theta) = \pi W\bar{S}(\theta)$ we have $S(\theta)|_{W\to 0} \sim \frac{6\pi W^2}{5T}$, which is consistent with the impulsive source case in (14).

A similar analysis applies to the correlation pattern in (29). Thus, for small W and θ

$$L(\theta) \simeq \begin{cases} 1 - \frac{3}{16}(\frac{6}{\pi})^{1/3}\ell^{-1/3}\bar{w}^{-1}\theta, & \theta < \Theta_{cL} \\ \frac{3}{2}\frac{W}{T(\theta)} \simeq \frac{3}{2}(\frac{\pi}{6})^{1/3}\ell^{1/3}\bar{W}\theta^{-1}, & \theta > \Theta_{cL} \end{cases} \tag{32}$$

Thus, comparing (32) and (30) we note that the energy and correlation patterns exhibit a similar behavior in the vicinity of the main beam direction for sources with $\bar{W} \ll 1$.

In summary, the results above support the conclusion obtained in connection with the peak-amplitude pattern $F_{\max}(\theta)$, namely, that in the quasi-impulsive limit flat broadside sources provide narrower beamwidth than elongated sources.

2) General Case: Simulation Results: Plots of $\bar{S}(\theta)$ for the length-to-width ratios $\ell = 100, 10, 1, 0.1$, and 0.01 and for the normalized square-pulse durations $\bar{W} = 0.1$ and $\bar{W} = 1.0$ are shown in Fig. 6(a) and (b). These plots are also very similar to those of $L(\theta)$ (not shown here). Referring to Fig. 4, we also find that $\bar{S}(\theta)$ [and, thus, $L(\theta)$, too] depends on θ, $\bar{W}$, and ℓ essentially in the same manner as the peak-amplitude pattern considered in Fig. 4. Furthermore, the numerical study also revealed that the 3-dB beamwidths of both $\bar{S}(\theta)$ and $L(\theta)$ depend on ℓ and $\bar{W}$ essentially in the same manner as the peak-amplitude beamwidth Θ_c considered in Fig. 5.

D. Pulse Duration and Range Resolution

The far-field pulse duration $\tau(\theta)$ is given by [see (21) and (22)]

$$\tau(\theta) = W + T(\theta) \tag{33}$$

where $T(\theta)$ of (11) is the pulse duration under impulsive excitation (i.e., $\tau|_{W=0} = T$). Plots of the normalized pulse duration $\bar{\tau}(\theta) \equiv \tau(\theta)c/V^{1/3}$ for various values of ℓ and $\bar{W}$ are shown in Fig. 7. Note that near the main-beam direction $\bar{\tau}(\theta)$ is mainly controlled by $\bar{W}$. The shape of the radiator (i.e., ℓ) has, on the other hand, a significant effect away from the main direction (for example, one can easily show that away from the main direction, $\bar{\tau}$ varies monotonically with θ *only* for $\ell \ge 1$).

3) Range Resolution for Highly Directive Sources: For highly directive sources we may consider only the angular range near the beam axis. Specifically, we shall consider the angular range $\theta < \Theta_c$ where Θ_c is peak amplitude beamwidth in (18), which provides a reasonable figure of merit to the relevant angular domain.

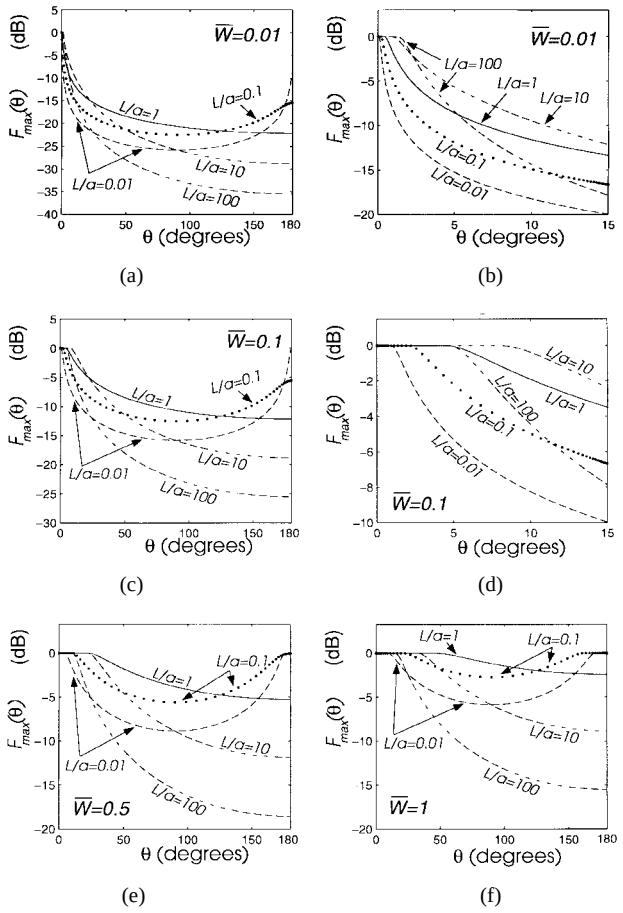

Fig. 4. Peak-amplitude pattern $F_{\max}$ versus θ for $\ell = 0.01, 0.1, 1, 10, 100$, and for various values of $\bar{W}$. (a) $\bar{W} = 0.01$. (b) Small angles behavior of (a). (c) $\bar{W} = 0.1$. (d) Small angles behavior of (c). (e) $\bar{W} = 0.5$. (f) $\bar{W} = 1.0$.

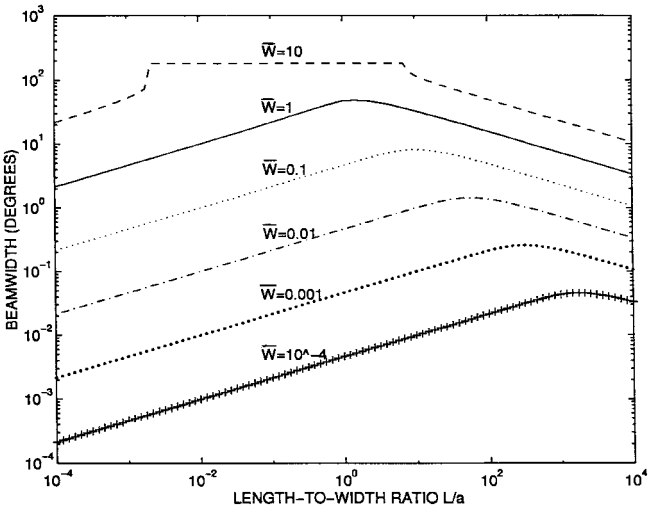

Fig. 5. Θ_c versus ℓ and parameterized by $\bar{W}$.

Using (33) together with (15) and (24) for small θ and Θ_c, the normalized pulse duration reduces to

$$\bar{\tau}(\theta) \simeq \bar{W} + (6/\pi)^{1/3}\ell^{-1/3}\theta = \bar{W}(1 + \theta/\Theta_c). \tag{34}$$

Next, we calculate the average pulse duration within the main-beam zone. Denoting this parameter as $\langle\bar{\tau}\rangle$ we find from (34)

$$\langle\bar{\tau}\rangle \equiv \frac{1}{\Theta_c}\int_0^{\Theta_c} d\theta\, \bar{\tau}(\theta) \simeq \frac{3}{2}\bar{W}. \tag{35}$$

Thus, for highly directive source distributions, $\langle\bar{\tau}\rangle$ is—apart from an unessential factor—equal to the normalized pulse width $\bar{W}$, thereby being independent of the source shape parameter ℓ.

A drawback of the above definition is that Θ_c depends both on ℓ and $\bar{W}$. Hence, the average value of the far-field pulse duration is computed within different angular regions for different source configurations. An alternative approach would be to measure the average of $\bar{\tau}$ within a fixed angular region $\theta \le \theta_0$ where θ_0 is some fixed small angle in the vicinity of the main direction. Analytical and computer-simulated results obtained for this case (not shown here) revealed that elongated sources provide better range resolution than planar sources of comparable size in the quasi-impulsive excitation case.

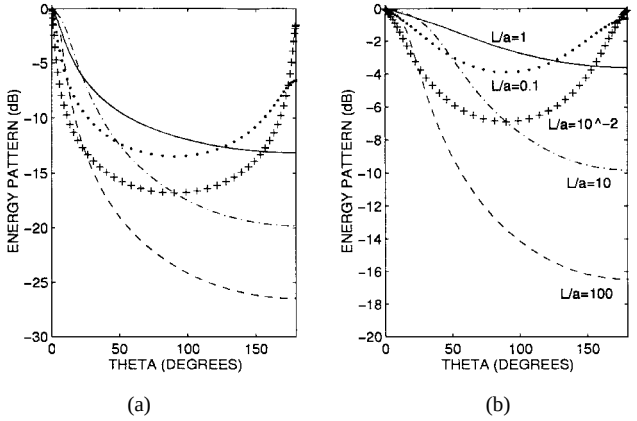

Fig. 6. Energy pattern $\bar{S}$ versus θ for $\ell = 0.01, 0.1, 1, 10, 100$, and for various values of $\bar{W}$. (a) $\bar{W} = 0.1$. (b) $\bar{W} = 1.0$.

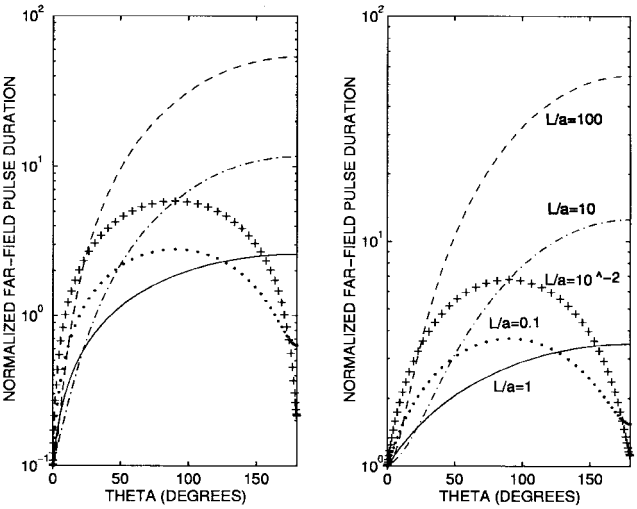

Fig. 7. Normalized far-field pulse duration $\bar{\tau}$ versus θ for $\ell = 0.01, 0.1, 1, 10, 100$, and for various values of $\bar{W}$. (a) $\bar{W} = 0.1$. (b) $\bar{W} = 1.0$.

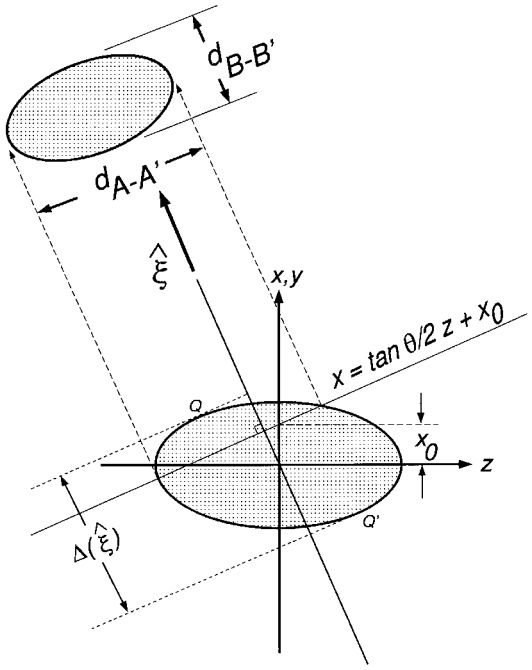

Fig. 8. Cross section of an ellipsoid volume source distribution used to compute the time-domain pulsed-radiation pattern $F_0(\hat{\mathbf{r}}, t)$ analytically.

V. Conclusion

This two-part sequence has dealt with the (far-field) radiation characteristics of collimated pulsed-source distributions having the "traveling-wave" form in (2). We have parameterized the radiation properties for sources of this class in both frequency and time domains. The time-domain route is based on radiation integrals in the form of planar projections of the time-dependent source distributions along the observation directions, thereby providing simple analysis and optimization tools with direct physical (geometrical) interpretation.

The general analysis tools were developed in the first paper. In that paper, we also considered explicitly the radiation characteristics of canonical parallelepiped source distributions under impulsive excitation. Such sources produce, however, singular field solutions along the main beam axis and, therefore, cannot be properly parameterized. This paper has considered finite duration signals. We studied, analytically, canonical source distributions with the shape of an ellipsoid whose axis coincides with the main-beam direction. Furthermore, by changing the ellipsoidal shape from a prolate to an oblate, we have clarified the different radiation characteristics obtained by an elongated quasi-linear traveling-wave source distribution or by a quasi-planar broadside source distribution.

We have been mainly concerned with the role both of the width of the excitation pulse and of the length-to-width ratio ℓ of the source for fixed-source volume. The source's focusing properties associated with the peak amplitude, energy, and "correlation" patterns were found to be strongly affected by both the excitation pulse width and the shape of the source. High directivity is achieved using either large planar ($\ell \ll 1$) or elongated ($\ell \gg 1$) sources and short-duration excitation pulses (such that $\bar{W} \ll 1$).

We also found that the angular dependence of all patterns studied (peak amplitude, energy, "correlation pattern," etc.) and, of the pulse duration, is monotonic only for $\ell \geq 1$ and that this result is independent of the normalized excitation pulse width $\bar{W}$. Planar broadside sources thus generate undesirable backward radiation lobes, which are not produced by elongated endfire sources.

We also explored the role of the length-to-width ratio on the directivity of the source when the normalized pulse duration is kept fixed. It was found that there is a breakdown region (or point $\ell = \ell_0$) where the beamwidth reaches its maximum (keeping $\bar{W}$ fixed). Optimal selection of the shape of the radiator is accomplished at any of the extremes $\ell \gg \ell_0$ or $\ell \ll \ell_0$ (i.e., choosing ℓ away from the breakdown region). Moreover, we have also investigated the variation of the suboptimal length-to-width ratio ℓ_0 as a function of the width of the excitation pulse. Interestingly, ℓ_0 was found to decrease *monotonically* with the normalized pulse width $\bar{W}$. Moreover, $\ell_0 \to \infty$ as $\bar{W} \to 0$. Hence, minimum beamwidth is accomplished in the quasi-impulsive excitation case by using the smallest possible value of ℓ (i.e., a planar source).

The range resolution in the neighborhood of the main-beam axis was found to be controlled mainly by the width of the excitation pulse. For highly directive sources (such as quasi-impulsively excited sources) the average range resolution as computed within the peak amplitude beam region $\theta \leq \Theta_c$ was found to be independent of the shape of the radiator.

Appendix

We refer to the geometry in Fig. 8, which schematically shows a cross section of the source in the direction $\hat{\boldsymbol{\xi}} = \cos\theta/2\hat{\mathbf{x}} - \sin\theta/2\hat{\mathbf{z}}$ where, without loss of generality, the $\hat{\boldsymbol{\xi}}$ axis is taken to be in the (x, z) plane. Denoting the point of intersection of the cross-sectional plane with the x axis as x_0 and the cross-sectional area by $A(\theta; x_0)$, we obtain from (6)

$$F_0(\theta, t) = \frac{c}{\xi} q_0 A(\theta; x_0)|_{x_0 \cos\theta/2 = -ct/\xi} \tag{36}$$

where, from (3), $q_0 = 1/V = \frac{6}{\pi a^2 L}$ and $\xi = 2\sin(\theta/2)$.

The line that delimits the cross section shown is a second-order polynomial with the shape of an ellipse with axes $d_{A-A'}$ and $d_{B-B'}$ given by

$$d_{A-A'} = \frac{L\sqrt{\mu(\theta) - 4x_0^2/a^2}}{\mu(\theta)\cos(\theta/2)} \tag{37}$$

$$d_{B-B'} = a\sqrt{\frac{\mu(\theta) - 4x_0^2/a^2}{\mu(\theta)}} \tag{38}$$

where $\mu(\theta) = 1 + \ell^2 \tan^2(\theta/2)$. The area of this ellipse is, therefore, given by

$$A(\theta; x_0) = \frac{\pi}{4} \frac{La\left[\mu(\theta) - 4x_0^2/a^2\right]}{[\mu(\theta)]^{3/2}\cos(\theta/2)}. \tag{39}$$

Substituting (39) in (36) yields (10). The peak amplitude is calculated using (8) with $A_{\max} = q_0 A(\theta; x_0 = 0) =$

$\frac{\pi}{4}\frac{La}{\cos\theta/2\sqrt{\mu(\theta)}}$, thus yielding

$$F_{0,\max}(\theta) = \frac{3c}{2\xi}\frac{1}{a\cos\theta/2\sqrt{\mu(\theta)}}. \tag{40}$$

The pulse duration is calculated using (7). The quantity $\Delta(\hat{\boldsymbol{\xi}})$ is obtained by finding the points Q and Q' in Fig. 8 where the ellipsoid is tangent to the plane $x = \tan\theta/2\ z + x_0$ and later computing the projection of the distance $Q - Q'$ in the direction $\hat{\boldsymbol{\xi}}$, giving $\Delta(\theta) = a\cos\theta/2\sqrt{\mu(\theta)}$.

REFERENCES

[1] E. A. Marengo, A. J. Devaney, and E. Heyman, "Analysis and characterization of ultrawideband scalar volume sources and the fields they radiate," *IEEE Trans. Antennas Propagat.*, vol. 45, pp. 1098–1106, July 1997.

[2] D. W. Liu, P. H. Carr, and J. B. Thaxter, "Nonlinear photoconducting characteristics of antenna activated by 80 picosecond optical pulses," *IEEE Photon. Technol. Lett.*, vol. 8, pp. 815–817, June 1996.

[3] D. W. Liu, J. B. Thaxter, and D. F. Bliss, "Gigahertz planar photoconducting antenna activated by picosecond optical pulses," *Opt. Lett.*, vol. 20, no. 14, pp. 1544–1546, July 1995.

[4] D. H. Auston, K. P. Cheung, and P. R. Smith, "Picosecond photoconducting hertzian dipoles," *Appl. Phys. Lett.*, vol. 45, no. 3, pp. 284–286, Aug. 1984.

[5] S. Mittlemann, P. Carr, and D. Liu, private communication, Rome Lab., Hanscom AFB, MA.

[6] H. F. Harmuth, "Antennas for nonsinusoidal waves: Part: III-Arrays," *IEEE Trans. Electromagn. Compat.*, vol. 25, pp. 346–357, Aug. 1983.

[7] A. Shlivinski, E. Heyman, and R. Kastner, "A unified antenna parameterization in the time and frequency domains," *IEEE Trans. Antennas Propagat.*, vol. 45, pp. 1140–1149, July 1997.

[8] J. D. Jackson, *Classical Electrodynamics*. New York: Wiley, 1962.

Edwin A. Marengo (M'89) was born in Panama City, Panama, in 1967. He received the Licenciado degree in electromechanical engineering (*summa cum laude*) from the Technological University of Panama, Panama City, and the M.S.E.E. and Ph.D. degrees from Northeastern University, Boston, MA, in 1990, 1994, and 1997, respectively.

From 1989 to 1990, he was a Teaching Assistant at the Department of Electrical Engineering, Technological University of Panama. From 1991 to 1992 he held positions as Mechanical Engineer at Asesores Técnicos e Industriales, Panama City, as Systems Engineering Trainee at IBM, Panama City, and as Adjunct Instructor of Applied Dynamics and Thermal Machines at the Technological University of Panama and of Electronics Laboratory and Electric Machinery at Universidad Santa Maria La Antigua, Panama City. From 1992 to 1997 he was with the Department of Electrical and Computer Engineering, Northeastern University, first as a Fulbright Scholar (1992–1994)—sponsored by the U.S. Government—and later as a Stipended Graduate Research Assistant. He is currently a Post-Doctoral Research Associate at the Center for Electromagnetics Research, Department of Electrical and Computer Engineering, Northeastern University. His main research interests include transient wave radiation and scattering, computational electromagnetics, and ground-penetrating radar imaging.

Dr. Marengo is a member of the IEEE Antennas and Propagation Society, Phi Kappa Phi, and Eta Kappa Nu.

Anthony J. Devaney (M'87), for photograph and biography, see p. 1106 of the July 1997 issue of this TRANSACTIONS.

Ehud Heyman (S'80–M'82–SM'88), for photograph and biography, see p. 528 of the May 1995 issue of this TRANSACTIONS.